

Measuring particle concentration in multiphase pipe flow using acoustic backscatter: Generalization of the dual-frequency inversion method

Hugh P. Rice,^{a)} Michael Fairweather, Timothy N. Hunter, Bashar Mahmoud, and Simon Biggs

School of Process, Environmental and Materials Engineering, University of Leeds, Leeds LS2 9JT, United Kingdom

Jeff Peakall

School of Earth and Environment, University of Leeds, Leeds LS2 9JT, United Kingdom

(Received 13 August 2013; revised 22 May 2014; accepted 23 May 2014)

A technique that is an extension of an earlier approach for marine sediments is presented for determining the acoustic attenuation and backscattering coefficients of suspensions of particles of arbitrary materials of general engineering interest. It is necessary to know these coefficients (published values of which exist for quartz sand only) in order to implement an ultrasonic dual-frequency inversion method, in which the backscattered signals received by transducers operating at two frequencies in the megahertz range are used to determine the concentration profile in suspensions of solid particles in a carrier fluid. To demonstrate the application of this dual-frequency method to engineering flows, particle concentration profiles are calculated in turbulent, horizontal pipe flow. The observed trends in the measured attenuation and backscatter coefficients, which are compared to estimates based on the available quartz sand data, and the resulting concentration profiles, demonstrate that this method has potential for measuring the settling and segregation behavior of real suspensions and slurries in a range of applications, such as the nuclear and minerals processing industries, and is able to distinguish between homogeneous, heterogeneous, and bed-forming flow regimes.

© 2014 Acoustical Society of America. [<http://dx.doi.org/10.1121/1.4883376>]

PACS number(s): 43.35.Bf, 43.30.Ft, 43.35.Yb [KGF]

Pages: 156–169

I. INTRODUCTION

Solid-liquid suspensions are ubiquitous, for example, in the nuclear, minerals, and chemical engineering industries, and the transport and mixing behavior of particles in turbulent, multiphase flows is of great practical and theoretical interest. In particular, the ability to measure the concentration of solid particles allows the operator to characterize many aspects of the flow and suspension properties, such as homogeneity or the presence of a moving or stationary bed that may cause a blockage or flow constriction, and the efficiency of mass transport and solids suspension by turbulent mixing. However, in situations where accessibility is difficult or chemical or radiological hazards are present, it is necessary to use remote measurement systems that are portable and simple to operate.

Diagnostic methods for the investigation of velocity and particle concentration fields in settling and nonsettling, multiphase suspensions can be categorized as follows (Bachalo, 1994; Powell, 2008; Shukla *et al.*, 2007; Williams *et al.*, 1990): external radiation (e.g., ultrasound, x rays, gamma rays, microwaves, optical light/lasers, neutrons); emitted or internal radiation (e.g., radioactive and magnetic tracers, NMR/MRI); electrical properties (e.g., capacitance, conductance/resistance, inductance and associated tomographic

methods, hot-wire anemometry); physical properties (e.g., sedimentation balance, hydrometric/density measurements, pressure, rheology); and direct methods (e.g., physical sampling, pumping, interruption). Consequently, a number of criteria must be considered when choosing the most appropriate measurement technique, such as potential hazards, physical size, ease of use and versatility, intrusiveness, cost, and the kind and accuracy of flow data that are required (Admiraal and García, 2000; Hultmark *et al.*, 2010; Laufer, 1954; Lemmin and Rolland, 1997; Povey, 1997). Acoustic instruments have many advantages over optical and other systems, most importantly their suitability for multiphase, sediment-laden, optically opaque flows, as well as their high mobility, ease of operation, low cost, low signal-processing, and calibration requirements and their ability to measure entire profiles, rather than make only single-point measurements.

Ultrasonic techniques can be used to study a range of processes (Povey, 2006), e.g., creaming, sedimentation, phase inversion and other phase transitions, and internal suspension properties, including volume fraction (as in this study), particle compressibility, and particle size (McClements, 1991; Povey, 2013). Such ultrasonic techniques utilize the speed of sound, attenuation and other, less commonly used ultrasonic properties, e.g., impedance, angular scattering profile (McClements, 1991), and are widely used in the study of colloidal suspensions (Challis *et al.*, 2005), marine sedimentary processes (Thorne and Hanes, 2002), and sedimentation and bed development in higher-concentration systems

^{a)}Author to whom correspondence should be addressed. Electronic mail: h.p.rice@leeds.ac.uk

(Hunter *et al.*, 2012a; Hunter *et al.*, 2012b; Hunter *et al.*, 2011). Indeed, Challis *et al.* (2005) are particularly keen to emphasize the benefits of ultrasonic methods, since one particularly useful capability of such methods is to interrogate suspensions of much higher concentrations than is possible with optical methods.

In this study, an acoustic model developed and used extensively by marine scientists (Thorne and Hanes, 2002; Thorne *et al.*, 2011) has been adapted in a novel way. The model relates the backscattered acoustic signal received by an active piezoelectric transducer to the properties of the particles in a suspension, and has been employed by a number of groups (Admiraal and García, 2000; Hunter *et al.*, 2012a). If the acoustic backscatter and attenuation coefficients of the suspension are known, then the particle concentration profile can be reconstructed using an explicit dual-frequency inversion method (Hurthier *et al.*, 2011), an extension of the former model that requires echo voltage profiles to be taken at two ultrasonic frequencies. However, published data for these acoustic coefficients only exist for quartz-type sand (Thorne and Meral, 2008). The adaptation presented here allows the backscatter and attenuation coefficients for suspensions of solid particles of any arbitrary material to be measured empirically, with the aim of applying the dual-frequency concentration inversion method to suspensions of engineering interest.

The objectives were to measure these coefficients directly for four particle species (two spherical glass, two nonspherical plastic), compare them to predicted values based on published quartz-sand data (Thorne and Meral, 2008), and construct concentration profiles in horizontal pipe flow in order to delineate various flow regimes and quantify the effects of particle concentration and size, and flow rate, on the segregation behavior of suspensions.

The structure of the paper is as follows: (a) scattering and absorption processes in insonified solid-liquid suspensions and an acoustic model for suspended particles are described in Sec. II, a novel modification of it for arbitrary types of particle is presented, and the dual-frequency inversion method is outlined; (b) the experimental method for measuring the attenuation and backscatter coefficients, and the physical properties of the particle species used, are described in Sec. III; and (c) some examples of particle concentration profiles calculated using the measured coefficients in horizontal pipe flow are presented in Sec. IV, in order to demonstrate the power of the technique as a whole.

II. THEORY

A. Acoustic scattering and absorption in suspensions of solid particles

The physical mechanisms present in an insonified suspension can be broadly divided into two types: (a) scattering, α_{sc} , and (b) absorption (i.e., conversion of acoustic energy into heat, sometimes referred to as dissipation). By analogy to optics, these two mechanisms collectively contribute toward attenuation (classically referred to as extinction) of the emitted signal in an additive fashion (Dukhin and Goetz, 2002). Absorption mechanisms can be categorized further, as follows (Babick *et al.*, 1998; Richter *et al.*, 2007): viscous

or visco-inertial, α_{vi} ; thermal, α_{th} ; structural, α_{st} ; electrokinetic, α_{el} ; and intrinsic, α_{in} or α_w , i.e., those mechanisms that are due to the liquid phase.

A broad summary of the various limiting cases in terms of particle size, ultrasonic wavelength and other parameters follows, where (Shukla *et al.*, 2010)

$$ka = \omega a/c = 2\pi f a/c = 2\pi a/\lambda, \quad (1)$$

with k the wave number, a the particle size, ω the ultrasonic angular frequency, c the speed of sound, f the ultrasonic frequency, and λ the wavelength. The long-, intermediate-, and short-wavelength (or Rayleigh, Mie, and geometric, by analogy to optical scattering) regimes correspond to $ka \ll 1$, $ka \sim 1$ and $ka \gg 1$ (or $\lambda \gg a$, $\lambda \sim a$, and $\lambda \ll a$), respectively. Several components of absorption can be neglected in the case of rigid, nonaggregating particles, as were used in this study. In particular, thermal (due to particle rigidity), structural (because there is no aggregation) and electrokinetic absorption are insignificant. Therefore, the total attenuation, α , is due to the following: intrinsic absorption in water, α_w ; viscous absorption, α_{vi} ; and scattering, α_{sc} (Richards *et al.*, 1996; Thorne and Hanes, 2002). So, $\alpha = \alpha_w + \alpha_s$, where the attenuation due to particles is $\alpha_s = \alpha_{sc} + \alpha_{vi}$.

Dukhin and Goetz (2002) note that “sub-micron particles do not scatter ultrasound at all in the frequency range under 100 MHz” but “only absorb ultrasound”; they also note that “absorption and scattering are distinctly separated in the frequency domain,” with absorption dominant at lower frequencies and scattering at higher frequencies. Babick *et al.* (1998) explain that in the long-wavelength regime (i.e., $ka \ll 1$), “scattering effects are negligible” and attenuation is mainly due to absorption. However, in the intermediate-wavelength regime (i.e., $ka \sim 1$), dissipation is negligible and “scattering, particularly by diffraction, increases enormously.”

Attenuation due to particles has generally been found to vary linearly with concentration at relatively low concentrations with a variety of particle types and fluids (Hay, 1983, 1991; Hunter *et al.*, 2012a; Richards *et al.*, 1996; Stakutis *et al.*, 1955). In early experiments, Urick (1948) observed a similar linear dependence, as did Greenwood *et al.* (1993) and Sung *et al.* (2008) using kaolin-water suspensions. Greenwood *et al.* concluded that scattering was insignificant in their experiments, since $\lambda \gg a$, and found that attenuation was directly proportional to volume fraction if “there is no interaction between particles.” Moreover, the relationship between attenuation and particle concentration has been found to remain linear over a greater range of concentration for lower values of ka (Carlson, 2002; Hay, 1991; Shukla *et al.*, 2010). At higher concentrations, however, the backscatter intensity becomes independent of concentration (Hay, 1991; Hipp *et al.*, 2002).

B. A model of acoustic backscatter strength

The model described by Thorne and Hanes (2002) and Thorne *et al.* (2011) for marine sediment was chosen for use in this study because it is simpler to implement than some

other, similar formulations (Carlson, 2002; Furlan *et al.*, 2012; Ha *et al.*, 2011) and has a firm theoretical basis (Hay, 1991; Kytömaa, 1995; Richards *et al.*, 1996). As a result, it has previously been employed by a number of groups (Admiraal and García, 2000; Hunter *et al.*, 2012a; Hurther *et al.*, 2011). In this section, the details of the model are described, with a view to developing it into a method for determining the properties of suspensions of arbitrary particles.

The backscattering and attenuation properties of the suspension are embodied in f , the backscatter form function, which “describes the backscattering characteristics of the scatterers” (Thorne and Buckingham, 2004), and χ , which is referred to by Thorne and Hanes (2002) as “the normalized total scattering cross-section.” The same authors state that the “sediment attenuation constant is due to absorption and scattering” which “for noncohesive sediments insonified at megahertz frequencies the scattering component dominates.” However, this can only be assumed to be true in the short-wavelength regime (i.e., at larger values of ka) and not in several of the suspensions used in the present study. For clarity, then, χ is hereafter referred to as the normalized total scattering and absorption cross-section. f and χ are proportional to $(ka)^2$ and $(ka)^4$ in the Rayleigh (i.e., long-wavelength) regime, and both tend to constant values at high values of ka .

The root-mean-square of the received voltage, V , varies with distance from the transducer, r , as follows:

$$V = \frac{k_s k_t}{\psi r} M^{1/2} e^{-2r\alpha}, \quad (2)$$

where $\alpha = \alpha_w + \alpha_s$, as described earlier; k_s is the sediment backscatter coefficient and incorporates the backscattering properties of the particles; k_t is a system parameter; M is the concentration by mass of suspended particles; and ψ is a

near-field correction factor (Downing *et al.*, 1995) that is written as follows:

$$\psi = \frac{1 + 1.35z + (2.5z)^{3.2}}{1.35z + (2.5z)^{3.2}}, \quad (3)$$

where $z = r/r_n$ and $r_n = \pi a_t^2 / \lambda$; a_t is the radius of the active face of the transducer; and λ is the ultrasound wavelength. ψ tends to unity in the far field, i.e., when $r \gg r_n$. α_s and k_s are as follows:

$$\alpha_s = \frac{1}{r} \int_0^r \xi(r') M(r') dr', \quad (4)$$

$$k_s = \frac{\langle f \rangle}{\sqrt{a \rho_s}}, \quad (5)$$

where ξ is the particle attenuation coefficient, given by

$$\xi = \frac{3\langle \chi \rangle}{4\langle a \rangle \rho_s}. \quad (6)$$

Angled brackets represent the average over the particle size distribution. In particular,

$$\langle f \rangle = \left(\frac{\langle a \rangle \langle a^2 f^2 \rangle}{\langle a^3 \rangle} \right)^{1/2}, \quad (7)$$

$$\langle \chi \rangle = \frac{\langle a \rangle \langle a^2 \chi \rangle}{\langle a^3 \rangle}. \quad (8)$$

Clearly, both k_s and ξ depend on the particle size distribution and shape and therefore distance from the transducer in the general case, as do M and α_s . Empirical expressions for f and χ are known for sandy sediment, i.e., quartz-type sand (Thorne and Meral, 2008) and are as follows:

$$f = \frac{x^2 \left(1 - 0.35 \exp \left[- \left(\frac{x - 1.5}{0.7} \right)^2 \right] \right) \left(1 + 0.5 \exp \left[- \left(\frac{x - 1.8}{2.2} \right)^2 \right] \right)}{1 + 0.9x^2}, \quad (9)$$

$$\chi = \frac{0.29x^4}{0.95 + 1.28x^2 + 0.25x^4}, \quad (10)$$

where $x = ka$, with k the ultrasonic wave number and a the particle radius.

No such data are available for particle species other than quartz sand, and it was beyond the remit of this study to construct equivalent expressions for other particle species. However, for the purpose of validation of the measured values presented later, estimates of the sediment attenuation coefficient, ξ , can be calculated for a particle species with a known density and mean size using Eqs. (6) and (10) by setting $a = d_{50}/2$ and $\langle \chi \rangle = \chi(x = ka)$, where d_{50} is the 50th percentile (i.e., median) of the measured particle size distribution (see Sec. IV A).

C. Determination of backscatter and attenuation coefficients in arbitrary suspensions

The objective in this section is to manipulate the expressions in the model presented in Sec. II B in order to derive expressions for the attenuation and backscatter coefficients, ξ_h and K_h , which are defined below and are measured in prepared homogeneous suspensions (hence the h subscript), that is, suspensions in which M is known and does not vary with distance. Measured values of ξ_h and K_h can then be used within the dual-frequency concentration inversion method (Hurther *et al.*, 2011), which is described in detail in Sec. II D, to construct concentration profiles in any homo- or heterogeneous suspension of the same particle species. The derivation is followed by a description of the experimental

method for measuring ξ_h and K_h in a stirred tank mixer and a summary of the measured values; last, those for ξ_h are compared to theoretical estimates of ξ and are discussed.

First, it is necessary to define the quantity G , the range-corrected echo amplitude, such that

$$G = \ln(\psi r V). \quad (11)$$

By multiplying both sides of Eq. (2) by ψr , taking the natural logarithm and then the derivative with respect to distance, r , the following expression is obtained:

$$\begin{aligned} \frac{\partial G}{\partial r} &= \frac{\partial}{\partial r} [\ln(\psi r V)] \\ &= \frac{\partial}{\partial r} \left[\ln(k_{sh} k_t) + \frac{1}{2} \ln M - 2r(\alpha_w + \alpha_{sh}) \right], \end{aligned} \quad (12)$$

where the h subscript signifies the specific case of homogeneity, which is necessary for the following stages of the derivation to be valid. This expression is similar to one given by Thorne and Buckingham (2004). Neither k_s , M nor α_s depend on r , so Eq. (4) can be simplified (i.e., $\alpha_{sh} = \xi_h M$, where ξ_h is the sediment attenuation constant in the case of a homogeneous suspension) and the first two terms on the right-hand side of Eq. (12) are zero. It can therefore be rewritten as follows:

$$\frac{\partial G}{\partial r} = -2(\alpha_w + \xi_h M). \quad (13)$$

So, the right-hand side of Eq. (13) varies linearly with M and this expression also provides a test for homogeneity. By taking the derivative with respect to concentration, an expression for ξ_h is obtained, as follows:

$$\xi_h = -\frac{1}{2} \frac{\partial^2 G}{\partial M \partial r} = -\frac{1}{2} \frac{\partial}{\partial M} \left[\frac{\partial}{\partial r} [\ln(\psi r V)] \right]. \quad (14)$$

This value of $\xi = \xi_h$ applies to a suspension in which the particle size distribution and concentration do not vary spatially. The quantity K is defined as the combined backscatter and attenuation constant, such that, in the general case

$$K \equiv k_s k_t = \psi r V M^{-1/2} \exp[2r(\alpha_w + \xi M)], \quad (15)$$

as described elsewhere (Betteridge *et al.*, 2008; Thorne and Buckingham, 2004; Thorne and Hanes, 2002). If ξ_h is known, it is then straightforward to find K_h , i.e., K measured in a homogeneous suspension according to the method described above, such that $K_h \equiv k_{sh} k_t$, for any combination of particle size and transducer frequency by evaluation of Eq. (15) which also requires that α_w , the attenuation due to water, be known. In this study, the expression given by Ainslie and McCollm (1998) was rewritten for the case of zero salinity, as follows:

$$\alpha_w = 0.05641 f^2 \exp\left(-\frac{T}{27}\right), \quad (16)$$

where α_w is in Np m^{-1} , f is the ultrasonic frequency in MHz and T is the temperature in $^\circ\text{C}$ ($6^\circ\text{C} < T < 35^\circ\text{C}$).

The method for determining the acoustic properties of suspensions of particles described in this section is novel and can be used with a very wide range of suspensions. Alternatively, any deviation from the expected behavior can be taken as an indication of heterogeneity, spatial variation in particle size distribution or significant attenuation.

D. The Hurther *et al.* dual-frequency concentration inversion method

Concentration inversion methods are algorithms that allow the particle concentration to be calculated by inversion of a suitable function that relates the concentration to some measured electromagnetic or acoustic property. They have found wide application in food, medical, and marine science but have not been exploited to the same extent by engineers, despite their practical and computational simplicity and low cost relative to other methods (e.g., tomography), and their ability to accurately monitor phase changes, identify critical transport velocities and delineate flow regimes, for example. In this section, a recent and very powerful acoustic inversion method is described, and concentration profiles in turbulent, horizontal pipe flow are constructed using backscatter and attenuation coefficients that were presented in Sec. IV A.

The explicit dual-frequency inversion method circumvents the inaccuracies associated with many other implicit and explicit methods that exhibit numerical instability in the far-field so that errors accumulate with distance from the transducer (Thorne *et al.*, 2011). With the dual-frequency method, the concentration can be calculated at any measurement point, independently of that at other points. A description of the method follows. Equation (2) can be rewritten for the general case, using Eq. (4), as follows (Hurther *et al.*, 2011; Thorne *et al.*, 2011):

$$V^2(r) = \Phi^2(r) J(r), \quad (17)$$

$$\Phi^2(r) \equiv \left(\frac{k_s k_t}{\psi r} \right)^2 e^{-4r\alpha_w} = \left(\frac{K}{\psi r} \right)^2 e^{-4r\alpha_w}, \quad (18)$$

$$J(r) \equiv M e^{-4 \int_0^r \xi(r') M(r') dr'} = V^2(r) / \Phi^2(r). \quad (19)$$

If the particle size distribution, and therefore ξ and k_s , do not vary with distance from the probe, which is a reasonable approximation if the particle species is neutrally buoyant, has a very narrow size distribution or is very well mixed, the exponent in Eq. (19) can be written as $-4\xi \int_0^r M(r') dr'$ [i.e., $\xi \neq \xi(r)$], and for two transducers that operate at different frequencies Eq. (19) can be rewritten as follows:

$$J_i(r) = M e^{-4\xi_i \int_0^r M(r') dr'}, \quad (20)$$

where $i = 1, 2$ for probes/frequencies 1 and 2 (i.e., 2 and 4 MHz in this study). Dividing Eq. (20) by M , then taking the natural logarithm and dividing both sides by ξ_i yields a constant right-hand side, such that

$$\left(\frac{J_1}{M}\right)^{\xi_2} = \left(\frac{J_2}{M}\right)^{\xi_1}, \quad (21)$$

and rearranging for M yields the following:

$$M^{\xi_1 - \xi_2} = J_1^{-\xi_2} J_2^{\xi_1}. \quad (22)$$

The explicit expression for particle mass concentration according to the dual-frequency inversion method is then obtained:

$$M = J_1^{(1-\xi_1/\xi_2)^{-1}} J_2^{(1-\xi_2/\xi_1)^{-1}}. \quad (23)$$

In the general case, the particle size distribution and detailed backscatter and attenuation properties are not known. Experimentally, J is evaluated by $J = V^2/\Phi^2$ via Eq. (19), where V is the measured voltage and Φ^2 is found using Eq. (18), which consists of the known variables in Eq. (2). Therefore, a minimal requirement for closure is that k_s and k_t (or K , as in this study), ξ and α_w are known. Whereas α_w can be calculated using Eq. (16), K and ξ must be determined experimentally.

The dual-frequency method requires that the particle scattering properties, and therefore, ξ_1 and ξ_2 differ so that M can be evaluated accurately from Eq. (23). However, this condition—which dictates that the smaller of the two frequencies lies in the Rayleigh (i.e., low- ka) regime in which ξ depends very strongly on ka , such that ξ_1/ξ_2 is “sufficiently different from unity” (Hurth et al., 2011)—is not so stringent in practice, and is easily satisfied for particles sizes of $a < 500 \mu\text{m}$ and frequencies in the range 1–5 MHz, because ξ is a strong function of ka . Indeed, it was found that the two frequencies used in this study, 2 and 4 MHz, were sufficiently different that the ratios of the measured values of ξ_1 to ξ_2 (i.e., ξ_{h1} and ξ_{h2}) at $f = 2$ and 4 MHz, respectively, for all four particle species differed significantly from unity (see results, Sec. IV).

III. MATERIALS AND METHODS

A. Materials

The acoustic properties of four particle species were investigated: “Honite 22” and “Honite 16” spherical glass particles, and “Guyblast 40/60” and “Guyblast 30/40” non-spherical plastic particles ($d_{50} = 41, 77, 468$ and $691 \mu\text{m}$,

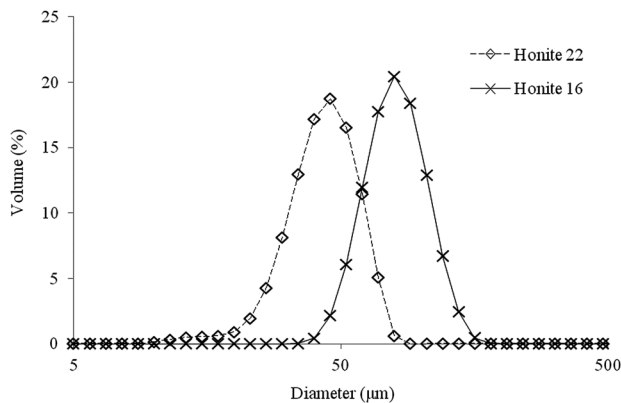


FIG. 1. Particle size distribution of Honite glass particle species. Data from *Mastersizer 2000*, Malvern Instruments.

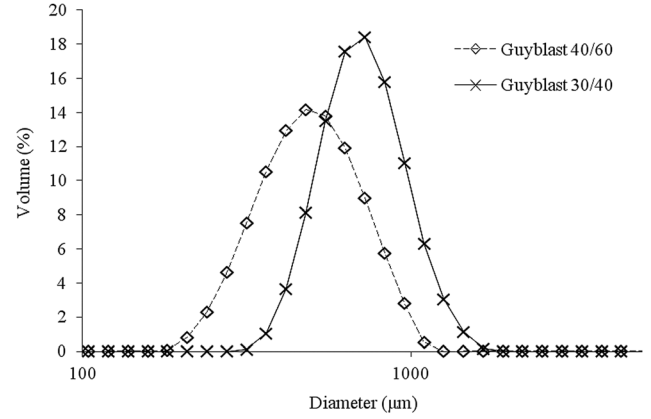


FIG. 2. Particle size distribution of Guyblast plastic particle species. Data from *Mastersizer 3000*, Malvern Instruments.

respectively). These species were chosen because they span a range of material properties—i.e., size distribution, density and shape—and therefore exhibit a range of acoustic scattering and absorption properties.

Particle size was measured with *Mastersizer 2000* and *3000* laser diffraction sizers (Malvern Instruments), density with an *AccuPyc 1300* pycnometer (MicroMeritics) and particle shape was confirmed by inspection of micrographs from a *BX51* optical microscope (Olympus). Measured particle size distributions for the glass and plastic species are given in Fig. 1 and Fig. 2, respectively. All particle properties are summarized in Table I.

B. Operation of the *UVP-DUO* acoustic backscatter system

As discussed in Sec. I, the capability of ultrasonic systems to interrogate suspensions with relatively high particle concentrations, along with the many other advantages described, formed the basis for the choice of the *UVP-DUO* ultrasonic signal processing unit (Met-Flow, Lausanne, Switzerland). This system was used with two ultrasonic emitter-receiver transducers operating at 2 and 4 MHz, as the principal diagnostic system in this study, as the objective was to investigate suspensions with particle concentrations of several percent by volume. Although intended to be used primarily as an ultrasonic Doppler velocimeter, the *UVP-DUO* is also a capable acoustic backscatter system and was used as such in this study: The voltage data themselves were used, rather than a Fourier transform of them, which yields the Doppler velocity (although the velocity field was used in the positional calibration of the probes, as described in Sec. IIID).

TABLE I. Physical properties of particle species. Species supplied by Guyson International, Ltd.

Species	Diameter, d_{50} (μm)	Density, ρ_s (10^3 kg m^{-3})	Shape
Smaller glass (Honite 22)	41.0	2.45	Spherical
Larger glass (Honite 16)	77.0	2.46	Spherical
Smaller plastic (Guyblast 40/60)	468	1.54	Jagged
Larger plastic (Guyblast 30/40)	691	1.52	Jagged

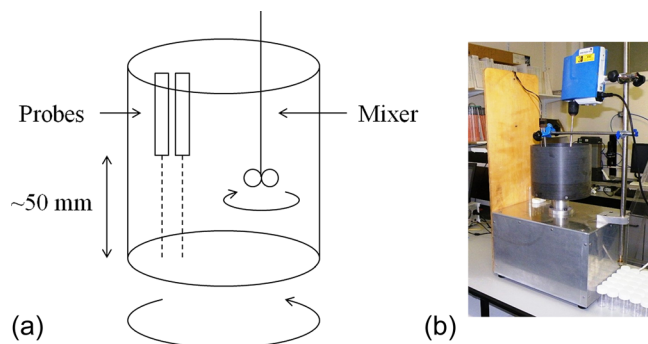


FIG. 3. (Color online) (a) Stirred mixing vessel schematic and (b) photograph. Mixing tank dimensions: 30 cm width, 30 cm depth. Probes were positioned at about 50 mm from, and perpendicular to, base.

In both the stirred mixing vessel and the pipe flow loop, described below, the two probes were attached to the *UVP-DUO* unit and excited at a voltage of 150 V. For each run, $n = 2500$ samples of the instantaneous received voltage were collected, with data from each transducer being taken separately in concurrent runs. Custom-written MATLAB scripts were used to process the data: The system-applied gain and digitization constants were removed, a three-sigma noise filter applied, and the root-mean-square (RMS) of the data was calculated to yield V [Eq. (2)].

C. Homogeneous suspensions in the stirred tank mixer

As described in Sec. II C, ξ_h and K_h are the values of ξ and K when measured in homogeneous suspensions according to the derivation described in Sec. II C. Such suspensions of known concentrations were prepared in the stirred mixing vessel shown in Fig. 3, which consists of a rotating plastic cylindrical container, the contents of which are mixed with an impeller connected to a high-speed mixer. Mains water (4 l) was used as the fluid at a total depth of around 10 cm. The probes were mounted below the water level in parallel, with active faces 5 cm from the base of the tank.

The suspensions were tested for homogeneity by taking physical samples (3 ml \times 60 ml samples at each concentration, as was the case for the main pipe flow loop described in more detail below) and comparing them to the total weighed concentration of solids. It was found that the suspensions prepared in the stirred mixing vessel were very uniformly mixed, with constants of proportionality between sampled and weighed concentrations for the Honite 22 (smaller glass), Honite 16 (larger plastic), Guyblast 40/60 (smaller

plastic), and Guyblast 30/40 (larger plastic) species of 0.998, 1.05, 0.987, and 0.863, respectively.

A range of nominal particle concentrations were used, from $\phi = 0.01$ to 10% by volume, which corresponds approximately to $M_w = 0.025$ to 250 kg m^{-3} for the two Honite glass species and $M_w = 0.015$ to 150 kg m^{-3} for the two Guyblast plastic species. However, attenuation was high in suspensions of Guyblast plastic particles at $M_w \geq 15 \text{ kg m}^{-3}$, and this limitation dictated the range over which the coefficients ξ_h and K_h were measured (see Sec. IV A).

D. Measurement of settling suspensions in horizontal pipe flow

Data were taken using the same two transducers mounted on a horizontal test section of a recirculating pipe flow loop (Fig. 4) with an inner diameter of $D = 42.6 \text{ mm}$ and a total capacity of 100 l (i.e., 0.1 m^3). A centrifugal pump, impeller mixer and electromagnetic flow meter were used. The probes were mounted at a distance $L = 3.2 \text{ m}$ (i.e., 75 D) from the nearest fitting to ensure the flow was fully developed (i.e., statistically invariant in the axial direction) at the test section, i.e., at a distance much larger than the necessary entrance length, even at the highest flow rates (Shames, 2003; Zagarola and Smits, 1998).

The flow loop was filled with suspensions of the same four particle species at several nominal (weighed) concentrations and run over a range of flow rates. Data from pairs of runs at the two ultrasonic frequencies were generated and combined (in which J_1 , J_2 , and M are functions of distance, r , from the transducer), and concentration profiles along a vertical cross-section were constructed using Eq. (23).

As shown in Fig. 4, the 2 MHz probe was mounted at 135° to the mean flow direction, and the 4 MHz probe at 90° , through a clasp on the pipe and through holes in the pipe wall. The positions of both probes were calibrated: (a) in the case of the 4 MHz probe, by reference to a strong peak in the echo amplitude corresponding to the position of the lower pipe wall; and (b) in the case of the 2 MHz probe, by reference to the position of the peak in the mean axial velocity profile (since the peak coincides with the pipe centerline at high flow rates), which was also measured. Because the probes were oriented at different angles to the flow direction, it was necessary first to perform a linear transformation of both datasets onto a common axis (for which the wall-normal distance, y , from the upper pipe wall was chosen). For the same reason, the measurement points for each

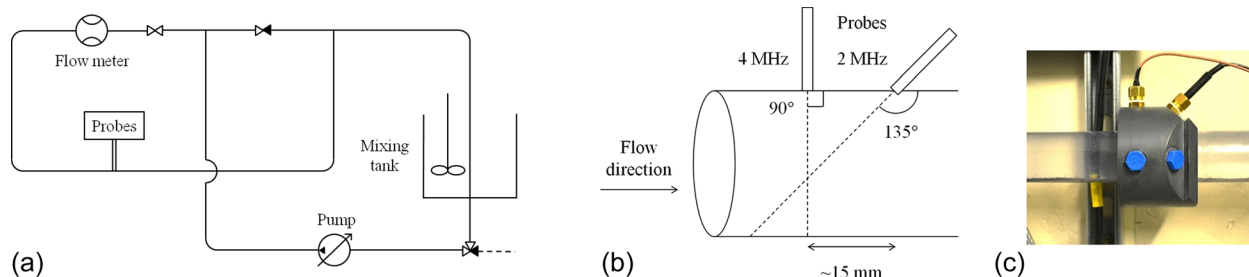


FIG. 4. (Color online) (a) Pipe flow loop schematic, (b) probe mounting geometry schematic and (c) photograph of probes attached to mounting clasp. Inner diameter, $D = 42.6 \text{ mm}$; entry length, $L = 3.2 \text{ m}$.

transducer were not co-located and so the data from the 2 MHz probe were interpolated linearly.

IV. RESULTS AND DISCUSSION

A. Measured coefficients and comparison with predictions based on quartz sand data

As specified in Eq. (14), in order to calculate ξ_h , it is necessary to know the gradient of G with respect to distance, r , and mass concentration, M . Echo voltage profiles were recorded using the *UVP-DUO* at several nominal mass concentrations with both transducers, which were aligned vertically in the stirred mixing vessel, and the data processed to yield the RMS echo voltage, V , from which G was calculated according to Eq. (11). Then, for each run, the gradient, $\partial G/\partial r$, was calculated over the region $r \approx 24$ to 46 mm because it was found that the variation in G tended to be most linear over this region, which was outside the near-field region at both frequencies, for all particles and at all concentrations of interest. Then, the gradient of $\partial G/\partial r$ with respect to M was found by compiling the results over a range of values of M according to Eq. (14).

Figure 5 shows G vs r with the 4 MHz probe for Honite 22, the smaller glass species, at low and high concentrations ($M_w = 2.41$ and 121.7 kg m^{-3}), for illustration of the goodness of fit. For conciseness, only data for the 4 MHz probe are shown, but the linear fits to the 2 MHz data were equally good. It should be noted that the peaked nonlinearities in the very near- and very far-field regions are assumed to be caused by flow around the tip of the probes ($r < 0.01 \text{ m}$) and reflection from the base of the stirred mixing vessel ($r > 0.05 \text{ m}$), respectively. The values of the gradient, $\partial G/\partial r$, over a range of concentrations are shown in Fig. 6 for both the 2 and 4 MHz probes. Gradients [from which ξ_h is calculated, via Eq. (14)] and goodness of fit with respect to weighed concentration, M_w , are also given. As can be clearly observed from Fig. 5, for example, G was found to vary very linearly with respect to r for all particle species over the

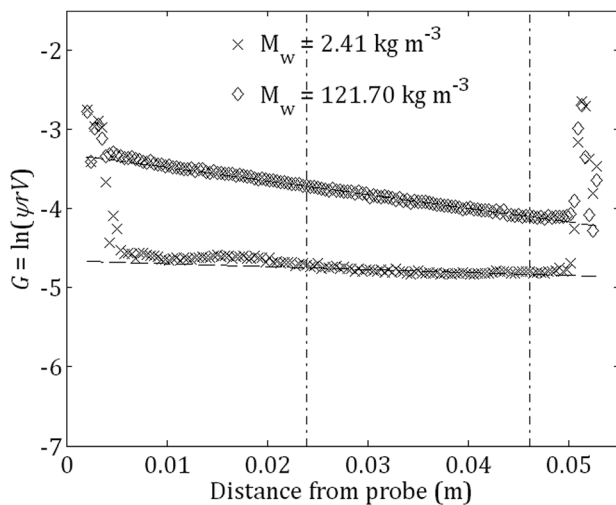


FIG. 5. G versus distance from 4 MHz probe with Honite 22 (smaller glass) at two nominal concentrations, $M_w = 2.41$ and 122 kg m^{-3} in stirred mixing vessel. Dashed lines through data are linear fits. Dot-dashed vertical lines indicate region over which gradients were calculated ($r \approx 24$ to 46 mm).

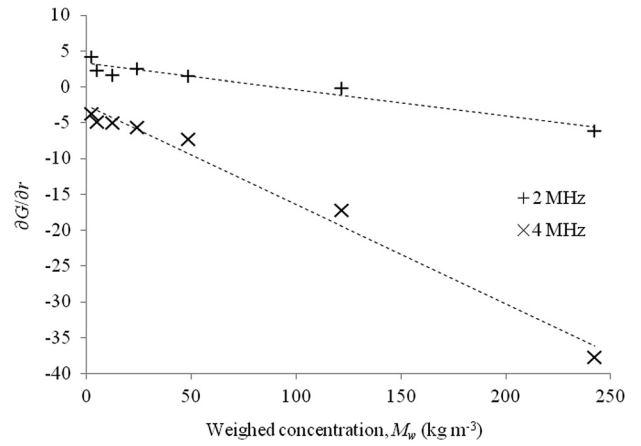


FIG. 6. Gradient of G with respect to distance from probe versus nominal mass concentration, M_w , of Honite 22 (smaller glass) in stirred mixing vessel at ultrasonic frequencies of $f = 2$ and 4 MHz. Goodness of fit for 2 and 4 MHz data was $R^2 = 0.932$ and 0.983 , respectively.

chosen region ($24 < r < 46 \text{ mm}$), as the model requires [Eq. (13)]. Moreover, the variation of $\partial G/\partial r$ with respect to M_w was also found to be highly linear for all particle species, as shown in Fig. 6, for example, as was also expected [Eq. (14)]. This kind of linear relationship between concentration and attenuation is well known (see Sec. II A).

Figure 7 and Fig. 8 show the same results but for the smaller plastic species (Guyblast 40/60). Similar trends are observed as for the glass particles, with a clear linear dependence of G on distance from probe, r , and in turn a clear linear dependence of $\partial G/\partial r$ on particle concentration. Collectively, these observations demonstrate two things: First, the success of the method as described, and second, that the suspensions in the stirred mixing vessel were, indeed, homogeneous (as linearity would not be expected in nonhomogeneous suspensions, as described in Sec. II C). Indeed, this method could be used as a simple test for homogeneity for a range solid-liquid suspensions in which such

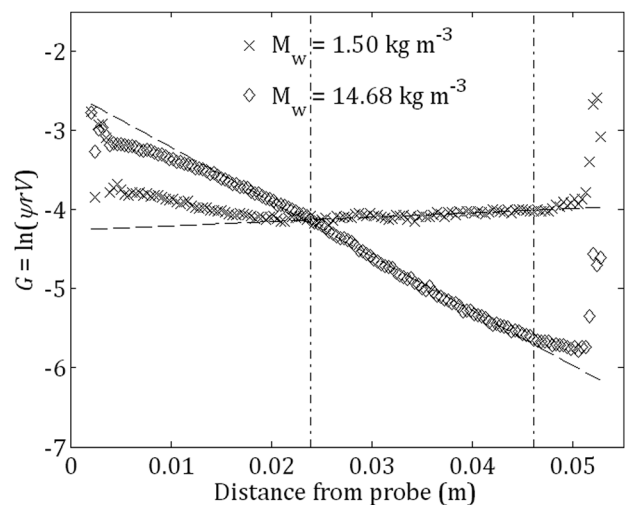


FIG. 7. G versus distance from 4 MHz probe with Guyblast 40/60 (smaller plastic) at two nominal concentrations, $M_w = 1.50$ and 14.7 kg m^{-3} in stirred mixing vessel. Dashed lines through data are linear fits. Dot-dashed vertical lines indicate region over which gradients were calculated ($r \approx 24$ to 46 mm).

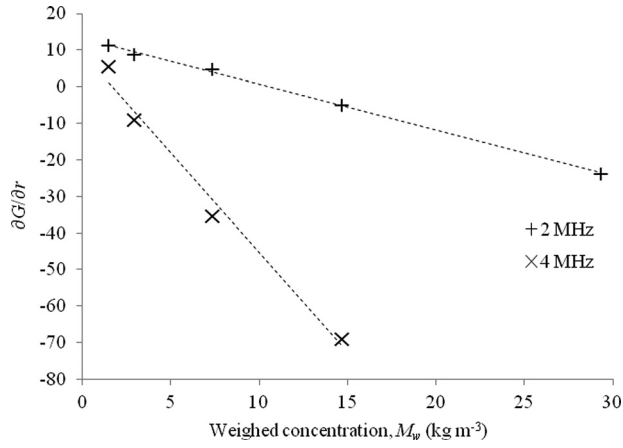


FIG. 8. Gradient of G with respect to distance from probe versus nominal mass concentration, M_w , of Guyblast 40/60 (smaller plastic) in stirred mixing vessel at ultrasonic frequencies of $f=2$ and 4 MHz. Goodness of fit for 2 and 4 MHz data was $R^2 = 0.999$ and 0.985, respectively.

conditions are to be maintained. However, it should be noted that $\partial G/\partial r$ could be calculated over a much smaller range of mass concentrations for the Guyblast plastic species than for the two Honite glass species. As is clear from Table II, in which the results for ξ_h are summarized, this difference can be accounted for by the fact that attenuation due to the plastic particles is much higher than for the glass, as would be expected, since the plastic particles are much larger.

Overall, then, the measured values of the attenuation coefficient, ξ_h , agree well with the predicted values, especially if the differences in material properties of the particle species are considered. The main conclusion to be drawn is that the degree of attenuation due to particles in the suspensions used, as quantified by the gradient of $\partial G/\partial r$, did indeed vary linearly with particle concentration, as was expected and as has been found by many other researchers (see Sec. II A).

The combined backscatter and system constant in the homogeneous case, K_h , was calculated according to Eq. (15) once the corresponding values of ξ_h were known, from the same runs. In every case, the mean values of K_h were calculated over the region $r \approx 24$ to 46 mm in order to be

TABLE II. Comparison of predicted and measured values of sediment attenuation constant, ξ_h , and combined backscatter and system constant, K_h . Values of ka are also given. (All results are given to three significant figures.)

Particle species	Honite 22	Honite 16	Guyblast 40/60	Guyblast 30/40
ka (2 MHz) ^a	0.174	0.327	1.99	2.93
ka (4 MHz) ^a	0.348	0.654	3.97	5.87
ξ_{h1} (2 MHz)				
Predicted ^b	0.00400	0.0242	0.953	1.01
Measured	0.0182	0.0212	0.627	1.34
ξ_{h2} (4 MHz)				
Predicted ^b	0.0570	0.274	1.807	1.44
Measured	0.0694	0.135	2.74	2.73
K_{h1} (2 MHz)	0.00229	0.00363	0.0100	0.0163
K_{h2} (4 MHz)	0.00430	0.00699	0.0239	0.0182

^aValue based on mean particle diameter, i.e., with $a = d_{50}/2$.

^bCalculated using Eqs. (6) and (10) by setting $a = d_{50}/2$ and $\langle \chi \rangle = \chi(x = ka)$.

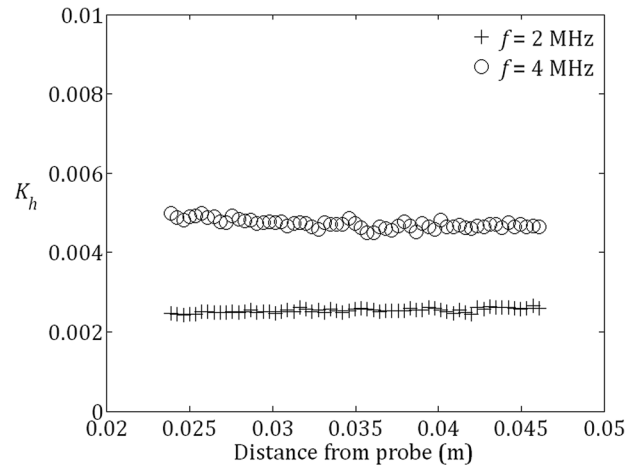


FIG. 9. Variation of combined backscatter and system constant, K_h , with distance from probe at $M_w = 12.2 \text{ kg m}^{-3}$ for smaller glass spheres (Honite 22) at ultrasonic frequencies of $f=2$ and 4 MHz in stirred mixing vessel. Relative standard deviations, $\sigma/\mu = 2.2\%$ and 2.4% .

consistent with the method of calculation of ξ_h . As a representative example and for illustration of the degree of variation with distance, Fig. 9 shows K_h versus distance with both the 2 and 4 MHz probes for Honite 22 (smaller glass) at an intermediate concentration ($M_w = 12.2 \text{ kg m}^{-3}$). Relative standard deviations are given in the caption. For conciseness, only data at one concentration are shown, but the data at other concentrations were equally good. The distance-averaged mean values of K_h for Honite 22 (smaller glass) are shown in Fig. 10 for both the 2 and 4 MHz probes. The equivalent results for Guyblast 40/60 (smaller plastic) are given in Fig. 11 and Fig. 12.

Concentration- and distance-averaged mean values of K_h for all particle species and both ultrasonic frequencies are summarized for all particle species in Table II for reference, along with predicted values of ξ , which were calculated via Eqs. (6) and (10), in which the measured values of the particle density and size were used (see Table I), i.e., $a = d_{50}/2$ and $\langle \chi \rangle = \chi(x = ka)$. (It was not possible to perform a similar comparison for K_h , as it contains a system constant, k_t , that could not be separated from the backscatter constant, k_{sh} ,

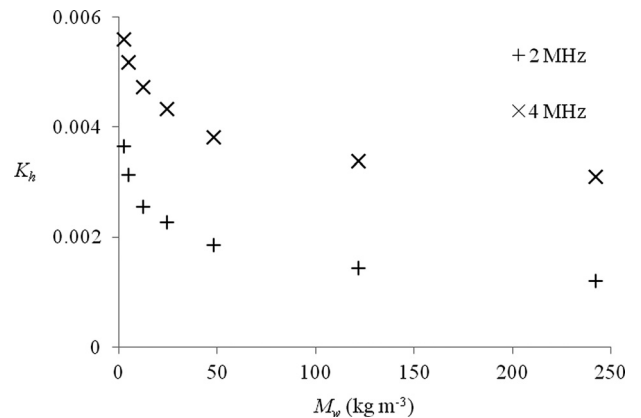


FIG. 10. Distance-averaged mean of combined backscatter and system constant, K_h , versus nominal mass concentration, M_w , for smaller glass spheres (Honite 22) at ultrasonic frequencies of $f=2$ and 4 MHz in stirred mixing vessel.

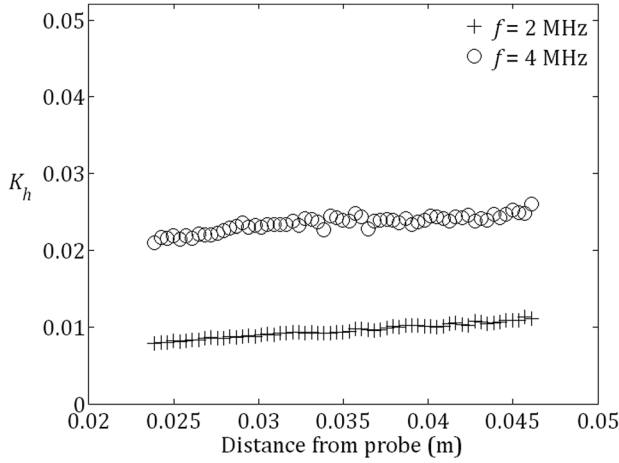


FIG. 11. Variation of combined backscatter and system constant, K_h , with distance from probe at $M_w = 7.38 \text{ kg m}^{-3}$ for smaller plastic particles (Guyblast 40/60) at ultrasonic frequencies of $f = 2$ and 4 MHz in stirred mixing vessel. Relative standard deviation, $\sigma/\mu = 9.4\%$ and 4.4% .

both being incorporated into K_h . Measuring k_t directly would require a more detailed knowledge of the electronics of the UVP-DUO instrument.)

Several of the expected trends in K_h were observed: K_h was found to be very constant with distance (the maximum spatial variation, as quantified by the relative standard deviation, μ/σ , was 9.4% for Guyblast 40/60 plastic at $f = 2 \text{ MHz}$; see Fig. 11); and the distance-averaged values of K_h increased with both particle size and ultrasonic frequency (except for the two Guyblast plastic species at $f = 4 \text{ MHz}$). However, for all particle species, K_h was found to vary with particle concentration, a result that was not expected, although the variation for the two Guyblast plastic species was less severe than for the two Honite glass species. The cause of this variation in K_h with concentration is not entirely clear, but the most probable cause is inaccuracies in ξ_h being propagated into K_h through Eq. (15): when calculated in this way, K_h is a strong (indeed, exponential) function of ξ_h . At higher values of ka , multiple scattering is likely to enhance attenuation, and therefore ξ_h and K_h , at higher concentrations, as is observed for Guyblast 40/60

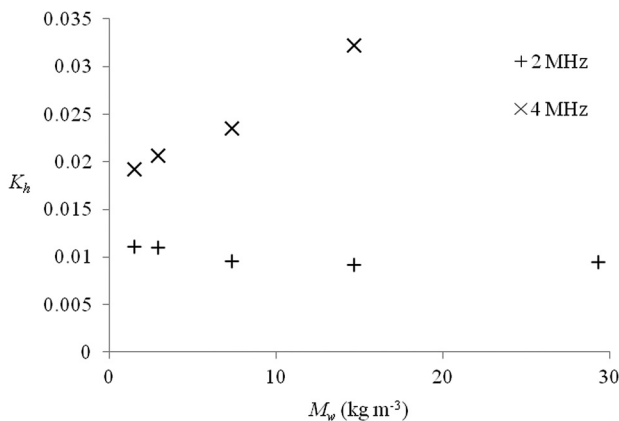


FIG. 12. Distance-averaged mean of combined backscatter and system constant, K_h , versus nominal mass concentration, M_w , for smaller plastic particles (Guyblast 40/60) at ultrasonic frequencies of $f = 2$ and 4 MHz in stirred mixing vessel.

(smaller plastic) at $f = 2 \text{ MHz}$, for example (Fig. 12). At lower values of ka , it may be that absorption becomes a significant contributor to attenuation, thereby enhancing K_h at lower concentrations, as was observed with Honite 22, the smaller glass species (Fig. 11) and as has been noted by Dukhin and Goetz (2002) in some particle types. Another possibility is that the calculated values of ξ_h and K_h were adversely affected by the fact that data were taken at logarithmic, rather than linear, intervals in the weighed concentration, M_w , thus giving undue weight to values at lower concentrations.

It is clear from Table II that the measured values of ξ_h are all within a factor of order unity of the predicted values. More generally, the measured values of both ξ_h and K_h increase with ka , as expected: in general, ξ and K are expected to be proportional to $(ka)^4$ and $(ka)^2$, respectively, at low ka (i.e., $ka \ll 1$) and approach constant values at high ka (i.e., $ka > 1$), where k is the ultrasonic wave number ($k = 2\pi/\lambda$) and a is the particle diameter (Thorne and Hanes, 2002). However, the discrepancies between the measured and predicted values of ξ_h are not insignificant, although this conclusion is likely less to be a failure of the mathematical and measurement techniques developed here, but to be due to the potential problems involved in estimating the acoustic properties of particles from the median value (i.e., d_{50}) of measured size distributions (Moate and Thorne, 2013; Thorne and Meral, 2008), and more generally due to the width of the particle size distributions.

Factors other than the particle size distribution are present, in particular: differences in density, compressibility and particle shape between the two spherical glass species (Honite) and the two nonspherical plastic species (Guyblast) and quartz sand data of Thorne and Meral (2008) that were used to predict ξ . Density is accounted for explicitly in the model, through Eqs. (5) and (6), and it is interesting to note that the density contrast between the fluid and solid phases influences the strength of visco-inertial scattering (Povey, 1997).

However, the influence of the remaining three factors—particle size distribution, particle shape and compressibility—is not accounted for explicitly in the model and is discussed below, in that order. First, the effect of width of the particle size distribution is assessed. Although not accounted for explicitly in the model, the size distribution is incorporated implicitly through Eqs. (9) and (10), which were determined empirically. In the Rayleigh regime (low ka), $\langle\chi\rangle/\chi > 1$, i.e., χ is underestimated; in the geometric regime (high ka), $\langle\chi\rangle/\chi < 1$, i.e., χ is overestimated; in addition, the discrepancy between predicted and measured values is larger for low ka and is proportional to the width of the particle size distribution, as quantified by $\kappa = \sigma/\langle a \rangle$ (Thorne and Meral, 2008), where $\langle a \rangle$ and σ are the mean and standard deviation of the particle size distribution, respectively. Therefore, measurements of ξ [which is related to χ through Eq. (6)] will be most sensitive to the width of the particle size distribution in the case of small, polydisperse species insonified at low frequencies. This trend is indeed observed in the results presented here: The measured values of ξ (i.e., ξ_h) at lower ka are generally lower than those predicted, and

higher than predicted at higher ka (see Table II), with the exception of Honite 22, the smaller glass species, at both ultrasonic frequencies. However, it is stressed that the accuracy of predicted values of ξ depends strongly on the polydispersity of the suspensions, which varies between species, as can be seen from Fig. 1 (Honite glass) and Fig. 2 (Guyblast plastic).

Second, particle shape is likely to have an effect on scattering and attenuation, and both the plastic species used here are highly nonspherical. According to Thorne and Buckingham (2004) in the geometric regime (i.e., at high ka) “a particle of irregular shape, having a similar volume to a sphere, would have a larger surface area and hence a higher geometric and scattering cross section,” and it is reasonable to assume that the backscattering and attenuation properties of highly irregular particles—that is, their ability to absorb and scatter energy—would be enhanced for the same reasons, since such particles present a larger projected surface area to the emitted acoustic beam than do spherical particles with the same volume. However, whether this enhancement of attenuation properties can fully account for the difference between the observed and predicted values at higher values of ka is left as a subject for further study.

Third, the compressibility of the particle species will inevitably affect their scattering and absorption properties. The strength of thermo-elastic scattering, which influences the strength of both backscattering and attenuation, is affected by the compressibility contrast between the liquid and solid phases (Povey, 1997) it is reasonable to conclude that this contrast is greater for suspensions of Honite glass particles than for Guyblast plastic particles, suggesting that compressibility is unlikely to be responsible for the differences between the measured and predicted values of the acoustic coefficients.

To summarize, the discrepancy between the measured and estimated values of ξ (and, for analogous reasons, K) can be accounted by a combination of the following: Differences in the physical properties of quartz sand and the species used in this study; and inaccuracies in the predicted values themselves, which are estimates based on the mean particle size, rather than entire size distributions. However, overall, the measured values of ξ_h and K_h demonstrate that the method as a whole was very successful. As stated earlier, such data only exist for quartz sand, and so one objective of this study—which was achieved—was to provide data for other kinds of particle species, in particular highly spherical glass (i.e., Honite) and highly nonspherical plastic (Guyblast). The ultimate aim, however, is to use the measured values of ξ_h and K_h to calculate concentration profiles in suspensions in arbitrary flow geometries of engineering interest via a dual-frequency inversion method (Hurther *et al.*, 2011), as described in the following section.

B. Implementation of the dual-frequency inversion method with measured acoustic coefficients in settling suspensions in horizontal pipe flow

To demonstrate the efficacy of the given method for the determination of the acoustic coefficients K_h and ξ_h , a series

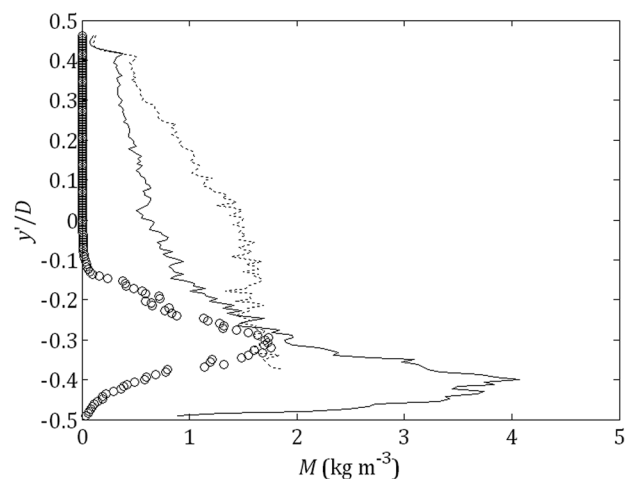


FIG. 13. Concentration by mass, M , versus reduced distance from center-line, y'/D , at three flow rates: $Q = 3.46, 1.71$, and 0.836 l s^{-1} and $M_s = 2.15, 1.14$, and 0.553 kg m^{-3} , respectively. Larger plastic particles (Guyblast 30/40 plastic, $d_{50} = 691 \mu\text{m}$), nominal mass concentration, $M_w = 1.50 \text{ kg m}^{-3}$ (nominal volume fraction, $\phi_w = 0.1\%$). Note that axes are inverted to aid visualization.

of measurements were completed in the pipe-flow loop to observe the settling behavior of flowing suspensions. By using the measured backscatter voltage, the parameter $J(r)$ was calculated for a particular distance r using Eq. (19) and $\Phi^2(r)$ using Eq. (18) according to the dual-frequency inversion method described in Sec. II D. The particle concentration, $M(r)$, through a vertical, wall-normal cross-section of the pipe could then be evaluated for a particular distance using Eq. (23) (where ξ_1 and ξ_2 are taken to be the measured values of ξ at 2 and 4 MHz, i.e., ξ_{h1} and ξ_{h2} , respectively, as given for each particle type in Table II). Some calculated concentration profiles for the large plastic and the large glass particle species are given in Fig. 13 and Fig. 14, respectively, for three different flow rates ($Q \approx 0.8$ to 3.5 l s^{-1}) and at different nominal bulk particle

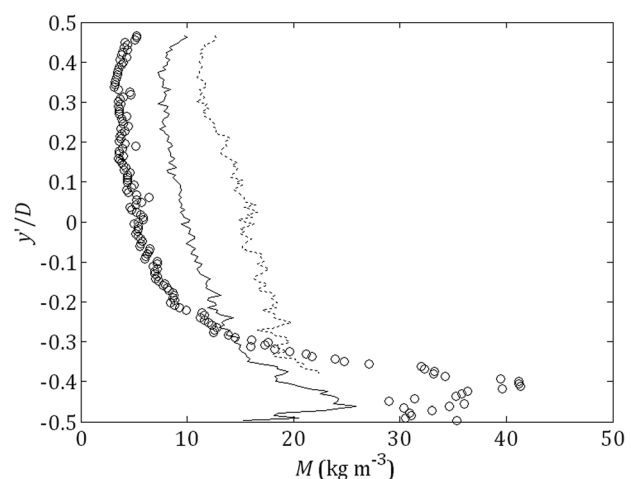


FIG. 14. Concentration by mass, M , versus reduced distance from center-line, y'/D , at three flow rates $Q = 3.50, 1.73$, and 0.850 l s^{-1} and $M_s = 26.6, 20.9$, and 10.9 kg m^{-3} , respectively. Larger glass particles (Honite 16 glass, $d_{50} = 77.0 \mu\text{m}$), nominal mass concentration, $M_w = 24.7 \text{ kg m}^{-3}$ (nominal volume fraction, $\phi_w = 1\%$). Note that axes are inverted to aid visualization.

concentrations ($M_w = 1.50 \text{ kg m}^{-3}$, $\phi_w = 0.1\%$ for plastic; $M_w = 24.7 \text{ kg m}^{-3}$, $\phi_w = 1\%$ for glass).

The three flow rates shown in Fig. 13 and Fig. 14 were chosen because they broadly correspond to three flow regimes: Pseudo-homogeneous, heterogeneous, and flow with a moving and/or stationary bed. It is clear from both sets of concentration profiles presented in Fig. 13 and Fig. 14 that at the highest flow rates ($Q \approx 3.5 \text{ l s}^{-1}$), the concentration gradient is closest to the nominal value through the pipe cross-section, although there is some variation with depth. Such a pseudo-homogeneous (rather than strictly homogeneous) flow is characteristic of a suspension in which the upward turbulent motions of the fluid are greater than the downward gravitational force on the solid particles. This competition is often quantified by the Rouse number, Ro , such that

$$Ro = w/\beta k u^*, \quad (24)$$

where w is the particle settling velocity, which depends on the particle size, shape, and density, β and k are constants such that $\beta \approx 1$ and $k \approx 0.4$, and u^* is the shear velocity (Allen, 1997). A low Rouse number signifies a fully suspended, well mixed suspension, whereas a high Rouse number signifies a settling suspension with a strong concentration profile.

However, at lower flow rates, M was found to increase more strongly with distance from the upper pipe wall, y —as would be expected for a real suspension of particles in which the downward force of gravity is comparable in magnitude to the force of the upward component of turbulent diffusion—signifying a highly heterogeneous flow, the most significant cause of which heterogeneity is depletion of the ambient concentration by deposition of particles in the mixing tank and along the lower pipe wall. There are clear peaks in M near the lower pipe wall in parts of Fig. 13 and Fig. 14, indicating strong settling (i.e., development of a significant concentration gradient). In fact, at the lowest flow rate in both Fig. 13 and Fig. 14, the region over which M was enhanced was sufficiently large that it is reasonable to assume a bed was present (which was confirmed visually). However, below the peaks, attenuation overwhelms the signal, and the method fails as the acoustic energy is absorbed by the bed.

The limiting concentration due to attenuation for the two Guyblast plastic species was $M = 15\text{--}20 \text{ kg m}^{-3}$ or so, whereas that for the two Honite (glass) species was at least $M = 150\text{--}200 \text{ kg m}^{-3}$. However, it is important to note that the attenuation appears to overwhelm the signal in the lowest part of the flow (Fig. 13 and Fig. 14) at concentrations lower than the limiting values. This is thought to be as a result of a number of factors: A very rapid increase in concentration in that region at lower flow rates, and the different acoustic path lengths from the frame of reference of each transducer, which were mounted at different angles to the flow (135° and 90° for the 2 and 4 MHz transducers, respectively).

Last, the observed differences between the two sets of concentration profiles are discussed, with reference to the physical properties of the two particle species. As would be

expected for a much smaller particle species, the concentration profiles for the glass species (Fig. 14) do not exhibit the same degree of heterogeneity as the plastic species (Fig. 13) at high and intermediate flow rates. In addition, at the lowest flow rates, the concentration of the plastic species is completely depleted in the upper region of the pipe due to settling [Fig. 13 and $0 < y \text{ (m)} < 0.025$], whereas much less significant depletion is observed in the glass suspensions.

The concentration profiles presented in this section demonstrate that the inversion method, implemented using measured acoustic coefficients, is able to accurately resolve the onset of the formation of settling in pipe flow and identify various flow regimes, i.e., homogeneous, heterogeneous, and settling/bed-forming flows.

An analysis of experimental errors, taking into account the effect of temperature, pressure, probe mounting angle and acoustic beam divergence, is presented in Rice (2013). For example, the lower limiting particle concentration at which temperature variations would cause errors in the attenuation due to water to be of a similar magnitude to the attenuation due to suspended particles is derived explicitly.

On the other hand, a full analytical error analysis of the calculated particle concentration, M , would be prohibitively long since M is a function of J_1 , J_2 , ξ_1 , and ξ_2 , where J_1 and J_2 are themselves functions of, and therefore subject to uncertainties in, K_1 , K_2 , α_{w1} , and α_{w2} (the subscripts 1 and 2 corresponding to frequencies 1 and 2, in this study 2 and 4 MHz). In the appendix, the influence of the uncertainty in one derived quantity, K_1 , on M is derived explicitly as an example. The analysis is restricted to K_1 for brevity, although it is important to note that M depends on four measured acoustic coefficients (K_1 , K_2 , ξ_1 , and ξ_2).

It is clear from Eq. (A10) (see Appendix) that there is a singularity in dM/M at $\xi_1/\xi_2 = 1$, with dM/M decreasing the further ξ_1/ξ_2 is from unity, and that dM/M depends strongly on the accuracy with which K_1 is calculated and is a constant for a particular particle species, i.e., both dK_1/K_1 and dM/M are independent of flow conditions and distance from the transducer. It is important to note that all these observations apply equally to dK_2 , and it is therefore reasonable to assume that the error in M due to dK_2 would be of a similar magnitude to that due to dK_1 .

The magnitudes of dK_1 and dM were computed for all four particle species. In this study, dK_1 was taken to be the standard error in the data used to calculate K_{h1} (see Fig. 10 and Fig. 12), which yielded values of the relative error dM/M [according to Eq. (A10)] of 40%, 49%, 11%, and 26% for the smaller glass (Honite 22), larger glass (Honite 16), smaller plastic (Guyblast 40/60), and larger plastic (Guyblast 30/40), respectively. The corresponding values of dK_{h1}/K_{h1} were found to be 15%, 21%, 4.1%, and 6.7%.

Using the analysis presented in the appendix, the error in M is plotted for two example runs at intermediate flow rates with Guyblast 30/40 (larger plastic) at $\phi_w = 0.1\%$ in Fig. 15(a) and Honite 16 (larger glass) at $\phi_w = 1\%$ in Fig. 15(b) (also shown without error bounds in Fig. 13 and Fig. 14), respectively.

It is important to assess whether the magnitude of the errors in K_{h1} and M are reasonable, since this is an indication

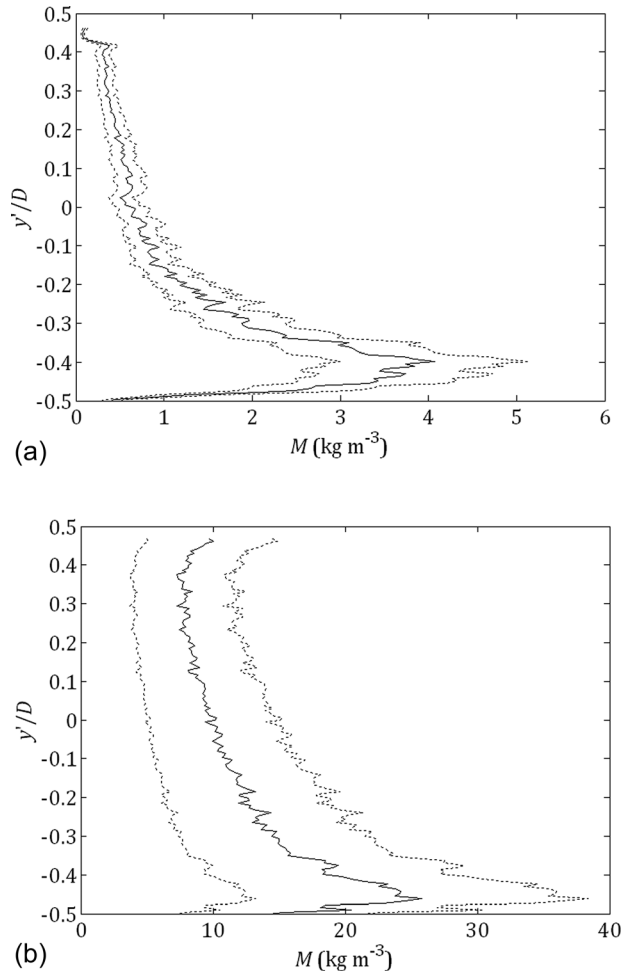


FIG. 15. Concentration by mass, M , versus reduced distance from centerline, y'/D , at intermediate flow rate (solid line), with error bounds, $\pm dM$, due to uncertainties in K_1 shown (dashed lines). (a) Larger plastic particles (Guyblast 30/40 plastic, $d_{50} = 691 \mu\text{m}$), $Q = 1.71 \text{ l s}^{-1}$, $\text{Re} = 51\,100$, $M_s = 1.14 \text{ kg m}^{-3}$, $M_w = 1.50 \text{ kg m}^{-3}$, $\phi_w = 0.1\%$; (b) larger glass particles (Honite 16 glass, $d_{50} = 77.0 \mu\text{m}$), $Q = 1.73 \text{ l s}^{-1}$, $\text{Re} = 51\,600$, $M_s = 20.9 \text{ kg m}^{-3}$, $M_w = 24.7 \text{ kg m}^{-3}$, $\phi_w = 1\%$. Note that axes are inverted to aid visualization.

of the accuracy of the method as a whole. Clearly, dK_1 ought to be minimized in general in order to minimize dM , since the former may be amplified in the latter through Eq. (A10), depending on the ratio of ξ_1 and ξ_2 . Since dM/M due to K_1 (and by analogy, K_2) does not vary with distance according to the analysis presented in the Appendix, the error in K_i cannot cause a divergence in M with distance in relative terms, as is observed with some other inversion methods, as shown by Hurther *et al.* (2011). Moreover, the observed variation in K_{h1} with respect to weighed mass concentration, M_w (see Fig. 10 and Fig. 12), although unexpected, is similar in magnitude to the scatter observed in the data for the acoustic coefficients f and χ compiled by Thorne and Meral (2008) from a variety of studies.

The variation in K_{h1} with M_w , and therefore in dK_{h1}/K_{h1} and dM/M , was higher for the Honite (glass) species was higher than for the Guyblast (plastic). Although this was to be expected since the variation in K_h with concentration was greater for the glass species (see Fig. 9), the physical reasons are not clear, but several possible causes exist: At low concentrations the effect of temperature variations on the attenuation due to water becomes more significant (Rice, 2013), whereas

at high concentrations the effect of absorption and multiple scattering are likely to dominate. It is also noted that the concentration range over which K_h was measured for the glass species was an order of magnitude larger than that for the plastic (because of lower attenuation) which is perhaps why greater variation was observed. Current studies (for future publication) are focused on assessing the most appropriate concentration range for each particle type when measuring ξ_h and K_h .

V. CONCLUSIONS

A model, described by Thorne and Hanes (2002) and Thorne *et al.* (2011), for which the acoustic properties of suspended particles have only been published for quartz-type sand, was adapted such that the attenuation and backscatter coefficients, ξ_h and K_h , for particles of arbitrary physical properties can be measured experimentally and used in a dual-frequency concentration inversion method (Hurther *et al.*, 2011). Coefficients for four particle species (two types of glass sphere with median diameters of $d_{50} = 44$ and $71 \mu\text{m}$, and two types of jagged plastic bead, $d_{50} = 468$ and $691 \mu\text{m}$) were measured. Concentration profiles in horizontal pipe flow, constructed using the measured coefficients, were presented at four nominal particle concentrations over a range of flow rates and particle concentrations. The novel method of measuring ξ_h and K_h was found to be very successful: Both the values of the coefficients and the structure of the resulting concentration profiles in pipe flow followed the expected trends.

It is thought that the method used in this study, which is novel as a whole and represents an entire program of development and application, from particle characterization to visualization of multiphase flow and settling behavior, has great potential in a range of engineering industries where *in situ* characterization of flowing or settling suspensions is required. The effects of settling and bed formation, for example, were clearly observed in the results. The main limitation appears to be strong attenuation, with limiting concentration due to attenuation for the two Guyblast plastic species of $M = 15\text{--}20 \text{ kg m}^{-3}$ or and at least $M = 150\text{--}200 \text{ kg m}^{-3}$ for the two Honite (glass) species.

Last, the error analysis presented here demonstrates that the accuracy of the concentration profiles calculated according to the proposed method depends strongly on the accuracy to which the values of the acoustic coefficients K (and therefore ξ , as K is calculated using ξ) can be measured.

It is intended that the results for the attenuation and backscatter coefficients, presented here for spherical glass and irregular plastic particles, will form the basis of a larger database of coefficients for sediments commonly encountered in a range of engineering industries, and one aim is to provide engineers and scientists with reference values of ξ and K —which depend strongly on particle size, density, and shape—for use in environments where access is not possible and physical samples cannot be taken.

ACKNOWLEDGMENTS

The present study is based on part of the Ph.D. thesis of H.P.R. (“Transport and deposition behavior of model slurries in closed pipe flow,” University of Leeds, 2013). The authors

wish to thank the Engineering and Physical Sciences Research Council for their financial support of the work reported in this paper under EPSRC Grant EP/F055412/1, “DIAMOND: Decommissioning, Immobilization and Management of Nuclear Wastes for Disposal.” The authors also thank Peter Dawson, Gareth Keevil, and Russell Dixon for their technical assistance, and Olivier Mariette at Met-Flow, Switzerland, for his advice and support.

APPENDIX

The influence on the calculated suspended particle concentration by mass, M , of the uncertainty in one variable, K_1 , upon which M depends is derived for the general case as an example. First, the expression for M [Eq. (23)] is rewritten in the following form:

$$M = AB, \quad (\text{A1})$$

where

$$A \equiv J_1^{(1-\xi_1/\xi_2)^{-1}} \quad (\text{A2})$$

and

$$B \equiv J_2^{(1-\xi_2/\xi_1)^{-1}}. \quad (\text{A3})$$

For this analysis, only the error due to K_1 , and therefore A , is considered, while those due to the variables that constitute B are neglected such that dM , the error in M , is

$$dM = dA \left| \frac{\partial M}{\partial A} \right|. \quad (\text{A4})$$

From inspection of Eq. (A1), it is found that

$$\frac{\partial M}{\partial A} = B. \quad (\text{A5})$$

By inspection of Eqs. (A2), (19), and (18), it can be seen that A is a function of J_1 , J_1 of Φ_1^2 , and Φ_1^2 of K_1 , respectively, so that the term dA in Eq. (A4) can be expanded as follows:

$$dA = dK_1 \left| \frac{\partial(\Phi_1^2)}{\partial K_1} \frac{\partial J_1}{\partial(\Phi_1^2)} \frac{\partial A}{\partial J_1} \right|. \quad (\text{A6})$$

The partial derivatives on the right-hand side of Eq. (A6) are given below.

$$\frac{\partial A}{\partial J_1} = (1 - \xi_1/\xi_2)^{-1} J_1^{(1-\xi_1/\xi_2)^{-1}-1} = (1 - \xi_1/\xi_2)^{-1} \frac{A}{J_1}, \quad (\text{A7})$$

$$\frac{\partial(\Phi_1^2)}{\partial K_1} = \frac{2K_1}{\psi^2 r^2} e^{-4r\alpha_w} = \frac{2}{K_1} \Phi_1^2, \quad (\text{A8})$$

$$\frac{\partial J_1}{\partial(\Phi_1^2)} = -\frac{V_1^2}{(\Phi_1^2)^2} = -\frac{J_1}{\Phi_1^2}. \quad (\text{A9})$$

By substituting these expressions into Eqs. (A4) and (A6) and simplifying, the following expression for dM/M , the relative error in M due to uncertainties in K_1 , is obtained as follows:

$$\frac{dM}{M} = \frac{dK_1}{K_1} \left| -2(1 - \xi_1/\xi_2)^{-1} \right|. \quad (\text{A10})$$

- Admiraal, D. M., and García, M. H. (2000). “Laboratory measurement of suspended sediment concentration using an Acoustic Concentration Profiler (ACP),” *Exp. Fluids* **28**, 116–127.
- Ainslie, M. A., and McColm, J. G. (1998). “A simplified formula for viscous and chemical absorption in sea water,” *J. Acoust. Soc. Am.* **103**, 1671–1672.
- Allen, P. A. (1997). *Earth Surface Processes* (Blackwell Science, Oxford, UK), 416 pp.
- Babick, F., Hinz, F., Stintz, M., and Ripperger, S. (1998). “Ultrasonic spectrometry for particle size analysis in dense submicron suspensions,” *Part. Part. Syst. Charact.* **15**, 230–236.
- Bachalo, W. D. (1994). “Experimental methods in multiphase flows,” *Int. J. Multiphas. Flow* **20**, 261–295.
- Betteridge, K. F. E., Thorne, P. D., and Cooke, R. D. (2008). “Calibrating multi-frequency acoustic backscatter systems for studying near-bed suspended sediment transport processes,” *Cont. Shelf Res.* **28**, 227–235.
- Carlson, J. (2002). “Ultrasonic characterization of materials and multiphase flows,” Ph.D. dissertation, Lulea University, Luleå, Sweden, 146 pp.
- Challis, R. E., Povey, M. J. W., Mather, M. L., and Holmes, A. K. (2005). “Ultrasound techniques for characterizing colloidal dispersions,” *Rep. Prog. Phys.* **68**, 1541–1637.
- Downing, A., Thorne, P. D., and Vincent, C. E. (1995). “Backscattering from a suspension in the near field of a piston transducer,” *J. Acoust. Soc. Am.* **97**, 1614–1620.
- Dukhin, A. S., and Goetz, P. J. (2002). *Ultrasound for Characterizing Colloids: Particle Sizing, Zeta Potential, Rheology* (Elsevier, Amsterdam, Netherlands), 382 pp.
- Furlan, J. M., Mundla, V., Kadambi, J., Hoyt, N., Visintainer, R., and Addie, G. (2012). “Development of A-scan ultrasound technique for measuring local particle concentration in slurry flows,” *Powder Technol.* **215–216**, 174–184.
- Greenwood, M. S., Mai, J. L., and Good, M. S. (1993). “Attenuation measurements of ultrasound in a kaolin-water slurry: A linear dependence upon frequency,” *J. Acoust. Soc. Am.* **94**, 908–916.
- Ha, H. K., Maa, J. P. Y., Park, K., and Kim, Y. H. (2011). “Estimation of high-resolution sediment concentration profiles in bottom boundary layer using pulse-coherent acoustic Doppler current profilers,” *Mar. Geol.* **279**, 199–209.
- Hay, A. E. (1983). “On the remote acoustic detection of suspended sediment at long wavelengths,” *J. Geophys. Res.* **88**, 7525–7542, doi:10.1029/JC088iC12p07525.
- Hay, A. E. (1991). “Sound scattering from a particle-laden, turbulent jet,” *J. Acoust. Soc. Am.* **90**, 2055–2074.
- Hipp, A. K., Storti, G., and Morbidelli, M. (2002). “Acoustic characterization of concentrated suspensions and emulsions. 2. Experimental validation,” *Langmuir* **18**, 405–412.
- Hultmark, M., Bailey, S. C. C., and Smits, A. J. (2010). “Scaling of near-wall turbulence in pipe flow,” *J. Fluid Mech.* **649**, 103–113.
- Hunter, T. N., Darlison, L., Peakall, J., and Biggs, S. (2012a). “Using a multi-frequency acoustic backscatter system as an in situ high concentration dispersion monitor,” *Chem. Eng. Sci.* **80**, 409–418.
- Hunter, T. N., Peakall, J., and Biggs, S. R. (2011). “Ultrasonic velocimetry for the in situ characterisation of particulate settling and sedimentation,” *Miner. Eng.* **24**, 416–423.
- Hunter, T. N., Peakall, J., and Biggs, S. (2012b). “An acoustic backscatter system for in situ concentration profiling of settling flocculated dispersions,” *Miner. Eng.* **27**:20–27.
- Hurth, D., Thorne, P. D., Bricault, M., Lemmin, U., and Barnoud, J.-M. (2011). “A multi-frequency Acoustic Concentration and Velocity Profiler (ACVP) for boundary layer measurements of fine-scale flow and sediment transport processes,” *Coast. Eng.* **58**, 594–605.
- Kytömaa, H. K. (1995). “Theory of sound propagation in suspensions—a guide to particle size and concentration characterization,” *Powder Technol.* **82**, 115–121.
- Laufer, J. (1954). “The structure of turbulence in fully developed pipe flow,” Report 1174 (National Bureau of Standards, Washington, DC), 18 pp.

- Lemmin, U., and Rolland, T. (1997). "Acoustic velocity profiler for laboratory and field studies," *J. Hydraul. Eng.* **123**, 1089–1098.
- McClements, D. J. (1991). "Ultrasonic characterization of emulsions and suspensions," *Adv. Colloid Interface Sci.* **37**, 33–72.
- Moate, B. D., and Thorne, P. D. (2013). "Scattering from suspended sediments having different and mixed mineralogical compositions: Comparison of laboratory measurements and theoretical predictions," *J. Acoust. Soc. Am.* **133**, 1320–1334.
- Povey, M. J. W. (1997). *Ultrasonic Techniques for Fluids Characterization* (Academic Press, San Diego, CA), 214 pp.
- Povey, M. J. W. (2006). "Acoustic methods for particle characterisation," *KONA* **24**, 126–133.
- Povey, M. J. W. (2013). "Ultrasound particle sizing: A review," *Particuology* **11**, 135–147.
- Powell, R. L. (2008). "Experimental techniques for multiphase flows," *Phys. Fluids* **20**, 040605.
- Rice, H. P. (2013). "Transport and deposition behaviour of model slurries in closed pipe flow," Ph.D. dissertation, University of Leeds, Leeds, UK, 270 pp. Available via White Rose eTheses Online: etheses.whiterose.ac.uk.
- Richards, S. D., Heathershaw, A. D., and Thorne, P. D. (1996). "The effect of suspended particulate matter on sound attenuation in seawater," *J. Acoust. Soc. Am.* **100**, 1447–1450.
- Richter, A., Voigt, T., and Ripperger, S. (2007). "Ultrasonic attenuation spectroscopy of emulsions with droplet sizes greater than 10 μm ," *J. Colloid Interface Sci.* **315**, 482–492.
- Shames, I. H. (2003). *Mechanics of Fluids* (McGraw-Hill, New York), 864 pp.
- Shukla, A., Prakash, A., and Rohani, S. (2007). "Particles settling studies using ultrasonic techniques," *Powder Technol.* **177**, 102–111.
- Shukla, A., Prakash, A., and Rohani, S. (2010). "Particle size monitoring in dense suspension using ultrasound with an improved model accounting for low-angle scattering," *AIChE J.* **56**, 2825–2837.
- Stakutis, V. J., Morse, R. W., Dill, M., and Beyer, R. T. (1955). "Attenuation of ultrasound in aqueous suspensions," *J. Acoust. Soc. Am.* **27**, 539–546.
- Sung, C. C., Huang, Y. J., Lai, J. S., and Hwang, G. W. (2008). "Ultrasonic measurement of suspended sediment concentrations: An experimental validation of the approach using kaolin suspensions and reservoir sediments under variable thermal conditions," *Hydrol. Process.* **22**, 3149–3154.
- Thorne, P. D., and Buckingham, M. J. (2004). "Measurements of scattering by suspensions of irregularly shaped sand particles and comparison with a single parameter modified sphere model," *J. Acoust. Soc. Am.* **116**, 2876–2889.
- Thorne, P. D., and Hanes, D. M. (2002). "A review of acoustic measurement of small-scale sediment processes," *Cont. Shelf Res.* **22**, 603–632.
- Thorne, P. D., Hurther, D., and Moate, B. D. (2011). "Acoustic inversions for measuring boundary layer suspended sediment processes," *J. Acoust. Soc. Am.* **130**, 1188–1200.
- Thorne, P. D., and Meral, R. (2008). "Formulations for the scattering properties of suspended sandy sediments for use in the application of acoustics to sediment transport processes," *Cont. Shelf Res.* **28**, 309–317.
- Urlick, R. J. (1948). "The absorption of sound in suspensions of irregular particles," *J. Acoust. Soc. Am.* **20**, 283–289.
- Williams, R. A., Xie, C. G., Bragg, R., and Amarasinghe, W. P. K. (1990). "Experimental techniques for monitoring sedimentation in optically opaque systems," *Colloid. Surface.* **43**, 1–32.
- Zagarola, M. V., and Smits, A. J. (1998). "Mean-flow scaling of turbulent pipe flow," *J. Fluid Mech.* **373**, 33–79.